ARTICLE

Synchrotron-Radiation Photoemission Study of Growth and Stability of Au Clusters on Rutile TiO_2(110)-1×1

Xin Yu[a], Ling-shun Xu[a], Wen-hua Zhang[b], Zhi-quan Jiang[a], Jun-fa Zhu[b], Wei-xin Huang[a]*

a. Hefei National Laboratory for Physical Sciences at the Microscale and Department of Chemical Physics, University of Science and Technology of China, Hefei 230026, China
b. National Synchrotron Radiation Laboratory, University of Science and Technology of China, Hefei 230029, China

(Dated: Received on April 30, 2009; Accepted on May 24, 2009)

The growth and thermal stability of Au clusters on a partially-reduced rutile TiO_2(110)-1×1 surface were investigated by high-resolution photoelectron spectroscopy using synchrotron-radiation-light. The valence-band photoelectron spectroscopy results demonstrate that the Ti^{3+}3d feature attenuates quickly with the initial deposition of Au clusters, implying that Au clusters nucleate at the oxygen vacancy sites. The Au4f core-level photoelectron spectroscopy results directly prove the existence of charge transfer from oxygen vacancies to Au clusters. The thermal stability of Au clusters on the partially-reduced and stoichiometric TiO_2(110) surfaces was also comparatively investigated by the annealing experiments. With the same film thickness, Au clusters are more thermally stable on the partially-reduced TiO_2(110) surface than on the stoichiometric TiO_2(110) surface. Meanwhile, large Au nanoparticles are more thermally stable than fine Au nanoparticles.

Key words: Synchrotron-radiation photoelectron spectroscopy, Au cluster, TiO_2(110), Charge transfer, Thermal stability

I. INTRODUCTION

Titania-supported Au nanoparticles have been demonstrated to exhibit unique catalytic performances in low temperature CO oxidation, selective oxidation of propene, and other oxidation reactions [1–9]. It has been found that the catalytic properties of supported gold nanoparticles strongly depend on the support and on the size and shape of Au nanoparticles, as well as other factors [9–12]. A general observation is the size-dependent catalytic activity of supported Au nanoparticles in low temperature CO oxidation. Finer supported Au nanoparticles are usually more active. However, the origin of the increased activity, that must be associated with the size-dependent geometric and electronic structures of Au nanoparticles, still remains ambiguous.

Model catalysts have been always employed for the fundamental understanding of heterogeneous catalysis. Regarding the supported Au catalysts, Au nanoparticles grown on a rutile TiO_2(110) surface (Au/TiO_2(110)) have been extensively investigated as the model catalyst, results greatly deepen our fundamental understanding of the structure-activity relationship of supported Au catalysts in low temperature CO oxidation. Valden *et al.* observed the same size-dependent catalytic activity in low temperature CO oxidation on the Au/TiO_2(110) model catalyst as that on powder Au/TiO_2 catalysts and found that a metal-to-nonmetal transition occurred for Au nanoparticles with a particle size of ∼3 nm [9]. Chen and Goodman successfully prepared extended Au films on TiO_x/Mo(112) and found that the Au bilayer exhibited an exceptionally high activity in low temperature CO oxidation [8]. The nucleation and growth of Au nanoparticles on TiO_2(110) have been experimentally investigated mainly using scanning tunneling microscopy (STM). Wahlström *et al.* reported that Au clusters preferentially nucleated on the bridging oxygen vacancies on TiO_2(110) and the combined density function theory (DFT) calculation showed that the adsorption energy of a single Au atom on a bridging oxygen vacancy site was more stable by 0.45 eV compared to that on the stoichiometric surface [13]. Matthey *et al.* observed different nucleation processes for Au clusters on reduced, hydrated, and oxidized TiO_2(110) surfaces and found that the adhesion of gold clusters is the strongest on the oxidized support [14]. The thermal stability of Au nanoparticles on TiO_2(110) has been considerably studied by STM [15–22]. The sintering of Au nanoparticles on TiO_2(110) occurs mainly by the Ostwald ripening mechanism [15–17], but in some cases particle diffusion/coalescence also occurs and might even dominate [17−20]. The electronic structure of Au clusters on

*Author to whom correspondence should be addressed. E-mail: huangwx@ustc.edu.cn, Tel.: +86-551-3600435, FAX: +86-551-3600437

TiO_2(110) has also been spectroscopically studied [23–27]. It is generally observed that the 4f binding energy of Au clusters deposited on TiO_2(110) exhibits a monotonic shift to high binding energy with the decreasing size, herein simply defined as particle size effect, whose origin, either from initial state effects or from final state effects, is still under argument [28].

The charge transfer between Au clusters and TiO_2(110) is an important and interesting issue. It is generally accepted that the charge transfer between the Au adatom and the stoichiometric TiO_2(110) substrate is negligible [29]. However, on the partially-reduced TiO_2(110) surface with bridging-oxygen vacancies, theoretical calculations have illustrated that significant charge transfer occurs from the titania support to the Au clusters [13,30–33]. The pronounced electron transfer from reduced TiO_2 to Au clusters was reported to greatly enhance the ability of Au clusters to catalyze CO oxidation [29,34]. DFT calculations [35] further demonstrated that the positively charged Ti at the Au/TiO_2 interface enhanced electron transfer from Au to the 2π orbitals of adsorbed O_2 to activate O_2 so that CO oxidation could occur at the interface via a CO(a)+O_2(a) mechanism with a very low barrier. Although the bridging-oxygen vacancies on TiO_2(110) have been found to markedly affect the geometric and electronic structures of deposited Au clusters and thus their catalytic properties [8–10,13,36,37], there is little direct evidence for the charge transfer from reduced TiO_2 to Au clusters. CO adsorption has been employed to probe the charge state of Au clusters supported on TiO_2(110) and the existence of electron-rich Au clusters was derived from the downward vibrational frequency shift of adsorbed CO [12,36,38]. Minato *et al.* studied the valence band of Au clusters on reduced TiO_2(110) and observed the shift of the O2p nonbonding peak and the attenuation in the Ti^{3+}3d peak with Au deposition, which was explained as a consequence of the electron transfer from the surface defects to Au clusters [24]. The core-level binding energy of metals is sensitive to their charge states, but due to the existence of particle size effect, the Au4f binding energy of Au clusters on TiO_2(110) failed to provide any information on the charge state of Au clusters. The Au4f binding energy was comparatively investigated for Au clusters deposited on the reduced and stoichiometric TiO_2(110) surfaces [25,27]. The Au4f binding energy shift was observed to be less on the reduced TiO_2(110) surface than that on the stoichiometric TiO_2(110) surface, which was taken as an indication of the involvement of initial state effect (charge transfer from Au to TiO_2) in the particle size effect; this also implied that the charge transfer from Au clusters to TiO_2 could be weakened by the existence of Ti^{3+} on the reduced TiO_2(110).

In our previous work [39], we employed X-ray photoelectron spectroscopy (XPS) to comparatively study the Au4f binding energy shift in the initial stage of Au growth on the reduced and stoichiometric TiO_2(110) surfaces and observed different size-dependent trends, which presented direct spectroscopic evidence for charge transfer from the defect sites on the reduced TiO_2(110) surface to Au clusters. In this work, high-resolution synchrotron-radiation photoelectron spectroscopy (SR-PES) was employed to investigate the initial growth of Au clusters on the reduced TiO_2(110) surfaces, results further confirmed the occurrence of charge transfer. Meanwhile, the thermal stability of Au clusters on the stoichiometric and reduced TiO_2(110) surfaces was also comparatively studied.

II. EXPERIMENTS

Experiments were performed on a VG multi-technique ultra high vacuum (UHV) system seated on the surface physics station of National Synchrotron Radiation Laboratory of China (Hefei, China). The photon energy could be tuned from 10 eV to 200 eV. The UHV system consisted of one analysis chamber and one preparation chamber between which the sample could be easily transferred. The analysis chamber had a base pressure of 8 nPa and was equipped with a hemisphere energy analyzer, conventional Al Kα and Mg Kα excitation sources, low energy electron diffraction (LEED) and a sputtering gun. The preparation chamber had a base pressure of 50 nPa and was equipped with facilities for the thin film deposition.

A TiO_2(110) single crystal (Princeton Scientific Corporation) was fixed on a molybdenum plate by two spot-welded Ta strips and introduced onto a sample stage in the analysis chamber through a fast entry lock. The sample stage could be heated by irradiation up to 1473 K by a hot W coil mounted backside, which heated the molybdenum plate and then the sample. The temperature of the sample stage was read out from a type K thermocouple, which was employed herein to indicate the sample temperature. However, the actual sample temperature was unknown and might be lower than the temperature of the sample stage. The sample was cleaned by standard procedures, including Ar^+ bombardment, oxidation and annealing, until LEED gave rise to a sharp TiO_2(110)-1×1 pattern and no contaminants could be detected by conventional XPS. The deposition of Au on TiO_2(110) was achieved in the preparation chamber by the physical evaporation of the high-purity Au (better than 99.99%) in a K-cell at 1473 K, which had been thoroughly degassed prior to its use. In our experiments, we employed a very slow evaporation rate of Au that was determined to be 0.40 Å/min by a thickness monitor TM400 from MAXTEK Inc. After deposition, the sample was quickly transferred to the analysis chamber for the synchrotron radiation photoelectron spectroscopy (SR-PES) measurements. The Au4f SR-PES spectra and the valence-band photoelectron spectra were measured with the photon energy of 150 and 28 eV, respectively. The Fermi level was de-

DOI:10.1088/1674-0068/22/04/339-345

termined using a thick Au layer. All the SR-PES features were calibrated as a reference of the synchrotron-radiation photon flux.

III. RESULTS AND DISCUSSION

The procedures for the reproducible preparation of clean stoichiometric and reduced TiO_2(110)-1×1 were firstly established. Figure 1 shows the valence-band photoelectron spectra of the sample at different stages. The clean TiO_2(110) sample was first bombarded at room temperature by Ar ions for 40 min and then vacuum-annealed at 873 K for 10 min, which was employed as the starting surface. A clear feature at approximately 0.75 eV below the Fermi level appears in the valence band photoelectron spectrum of the starting surface (Fig.1(a)), demonstrating the coexistence of various low-valence Ti cations [40,41]. No LEED pattern could be observed for the starting surface. The starting surface was then oxidized at 873 K for 40 min in 2 mPa oxygen ambient followed by vacuum-annealing at 1373 K for 10 min to order the surface, and a feature at approximately 0.9 eV below the Fermi level appears (Fig.1(b)), corresponding to the Ti^{3+}3d photoemission. The surface was oxidized again at 873 K for 30 min in 2 mPa oxygen and then vacuum-annealed at 873 K for 10 min. This treatment lead to an ordered and stoichiometric TiO_2(110) surface, whose valence-band photoelectron spectrum (Fig.1(c)) gives no feature for Ti^{3+}. Further vacuum-annealing of the ordered and stoichiometric TiO_2(110) surface at 1173 K results in the ordered and reduced TiO_2(110) surface, as evidenced by Ti^{3+}3d feature in the valence-band photoelectron spectrum (Fig.1(d)). The TiO_2(110) surfaces corresponding to the Fig.1 (c) and (d) both give rise to a sharp (1×1) LEED pattern (the inset of Fig.1), and thus are denoted as s-TiO_2(110) and r-TiO_2(110), respectively.

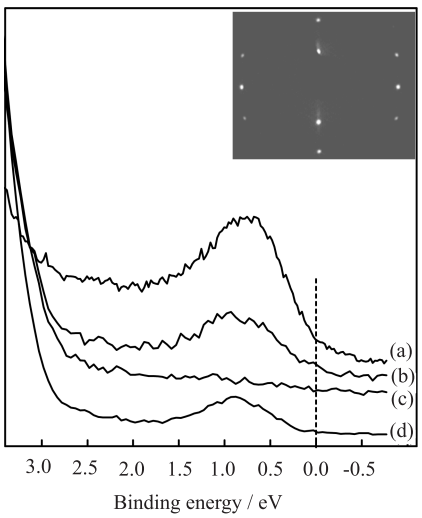

FIG. 1 The valence-band photoelectron spectra of (a) a clean rutile TiO_2(110) surface subjected to Ar^+ bombardment at room temperature for 40 min followed by vacuum-annealing at 873 K for 10 min, (b) the surface of (a) was oxidized at 873 K for 40 min in 2 mPa oxygen ambient followed by vacuum-annealing at 1373 K for 10 min, (c) the surface of (b) was oxidized again at 873 K for 30 min in 2 mPa oxygen followed by vacuum-annealing at 873 K for 10 min, (d) the surface of (c) was further vacuum annealed at 1173 K for 10 min. The inset shows a typical sharp (1×1) LEED pattern acquired for surfaces of (c) and (d) (E_p=110 eV).

Figure 2 presents a series of measured and fitted Au4f core level spectra after the deposition of Au films on the r-TiO_2(110) surface with different film thicknesses. The curve-fitting of the Au4f feature was performed by means of XPSPEAK 4.1 software package, with subtraction of a Shirley background. The Au film with the thinnest thickness of 0.1 Å exhibits a broad Au4f feature with the $4f_{7/2}$ component centered at 84.57 eV. The Au4f binding energy moves toward lower binding energy with increasing Au film thickness, with the $Au4f_{7/2}$ component at 84.17 eV for the Au film with a thickness of 1.5 Å. However, the $Au4f_{7/2}$ binding energy shifts unexpectedly from 84.17 eV to 84.21 eV when the Au film thickness increases from 1.5 Å to 1.7 Å. The $Au4f_{7/2}$ binding energy is 84.20 eV for the Au film with a thickness of 2.0 Å, and then shifts downward again with further increasing Au film thickness. The thickest Au film (10.0 Å) under the current study exhibits the $Au4f_{7/2}$ component at 84.07 eV. The Au4f feature gains its intensity monotonically with increasing Au film thickness.

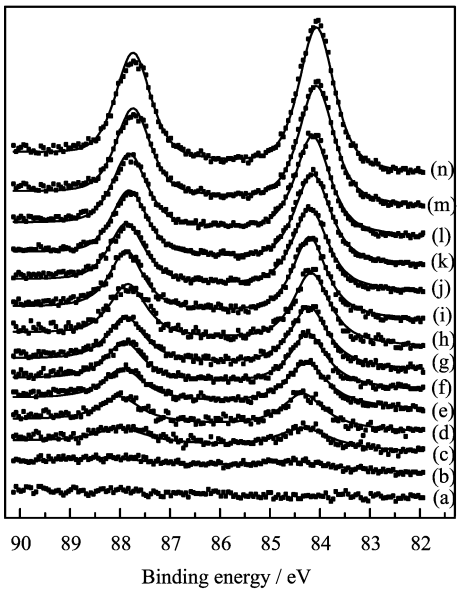

FIG. 2 The Au4f SR-PES spectra for Au deposition at room temperature on the r-TiO_2(110) surface with the Au thickness of 0, 0.1, 0.3, 0.5, 0.7, 1.0, 1.2, 1.5, 1.7, 2.0, 2.5, 3.0, 5.0, and 10.0 Å for (a)–(n), respectively. Scatter points and solid lines are experimental data and fitted curves, respectively. The incident photon energy was 150 eV.

DOI:10.1088/1674-0068/22/04/339-345

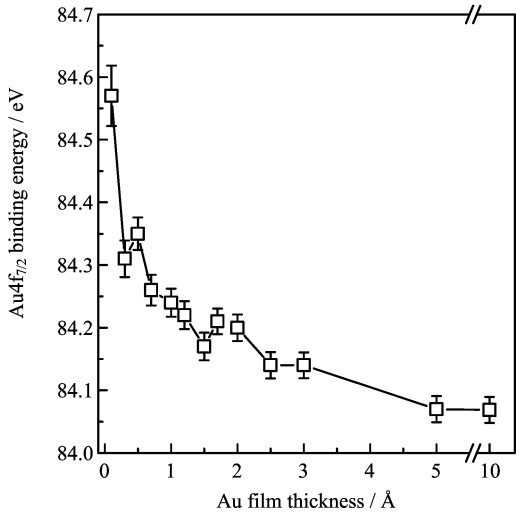

FIG. 3 The $Au4f_{7/2}$ binding energy as a function of the deposited Au film thickness on the r-TiO_2(110) surface. The incident photon energy was 150 eV.

Figure 3 illustrates the $Au4f_{7/2}$ binding energy as a function of Au film thickness. Repeated experiments showed that the $Au4f_{7/2}$ binding energy of Au films deposited on r-TiO_2(110) with the same thickness varied within 0.02 eV. The overall trend is that the Au4f binding energy of Au film decreases with the increasing film thickness, but an inverse of the Au4f binding energy shift is clear for the Au film thickness range between 1.5 and 2.5 Å. An inverse of the Au4f binding energy shift was also observed for Au film thickness from 0.3 Å to 0.5 Å (Fig.3). However, due to the very low Au coverage on r-TiO_2(110), the Au4f features of Au film with thicknesses of 0.3 and 0.5 Å have a poor signal-to-noise ratio (Fig.2). These two inverse binding energy shifts likely arise from the same physical origin. Therefore, we only focus on the inverse binding energy shift with Au thickness between 1.5 and 2.5 Å, whose Au4f features have nice signal-to-noise ratios. The SR-PES results of Au films deposited on r-TiO_2(110) agree very well with our previous results obtained by conventional XPS [39]. The Au4f SR-PES spectra presented herein are with the full width at half-maximum (FWHM) around 0.9 eV whereas those measured by conventional XPS are with the FWHM in the range of 1.3−1.9 eV [39].

The particle size effect observed for Au growth on stoichiometric TiO_2(110) [23–27] and SiO_2 [23,42] in which the 4f binding energy of Au clusters exhibits a monotonic shift to lower binding energy with the increasing size cannot solely explain the observed Au4f binding energy shift of Au clusters on r-TiO_2(110). There should be other factors. A reasonable model is that the particle size effect and the charge transfer from the bridging oxygen vacancies on r-TiO_2(110) to Au clusters cooperatively determine the Au4f binding energy shift of Au clusters on r-TiO_2(110). Resulting from the particle size effect, the $Au4f_{7/2}$ binding energy shifts to lower binding energy with the increasing size of Au clusters, and the particle size effect will disappear beyond a critical size d_1; therefore, the electronic properties of Au nanoparticles larger than d_1 approach to those of the bulk Au, and they exhibit the same Au4f feature as the bulk Au. On the other hand, the charge transfer from the bridging oxygen vacancies on r-TiO_2(110) makes Au clusters negatively charged and thus reduces the Au4f core level binding energy. Because the transferred charge from an bridging oxygen vacancy on oxide supports to the Au cluster are mainly localized to the interacting atom and the nearest neighbors [43], the charge transfer effect is most pronounced when Au atoms nucleate on the bridging oxygen vacancies on r-TiO_2(110) and will weaken with the increasing size of Au clusters. We define as d_2 the critical size of Au cluster beyond which the charge transfer no longer occurs for newly added Au atoms. Reasonably, d_2 is much smaller than d_1. Therefore, both the particle size and the charge transfer affect the Au4f binding energy for Au clusters with the size finer than d_2; only the particle size effect exists for Au clusters with the size between d_2 and d_1; the Au clusters with the size larger than d_1 exhibit the same electronic structure as the bulk Au. On the basis of this model, for Au clusters on r-TiO_2(110) finer than d_2, the Au4f binding energy is lower than that of Au clusters with the same size on s-TiO_2(110) and reduces monotonically with the increasing size of Au clusters; when the Au cluster's size reaches d_2, its Au4f binding energy should reasonably shift to higher binding energy due to the disappearance of the charge transfer effect on the newly-added Au atoms on the cluster; after that the Au4f binding energy of Au clusters reduces monotonically with the increasing cluster size again until reaching the value of bulk Au. Therefore, the model predicts that an inverse in the Au4f binding energy shift with the increasing size of Au cluster should exist for the Au deposition on r-TiO_2(110). Our SR-PES results, together with the previous XPS results [39], adequately support the prediction and thus provide strong evidence for the charge transfer from the bridging oxygen vacancies on r-TiO_2(110) to Au clusters.

The valence-band photoelectron spectra for Au/r-TiO_2(110) with different Au film thicknesses are shown in Fig.4. The clean r-TiO_2(110) surface exhibits a clear photoemission feature at approximately 0.9 eV below the Fermi level, corresponding to the Ti^{3+}3d occupied state. The Ti^{3+}3d peak attenuates greatly after the deposition of 0.1-Å-thick Au film. Inferred from the position and shape of this peak, the Ti^{3+}3d peak almost vanishes after the deposition of 0.3-Å-thick Au film. Instead, the remaining feature should arise from the photoemission of 6s electrons of Au clusters. The titration of the Ti^{3+}3d peak by Au deposition has been previously observed for Au growth on a reduced TiO_2(110) surface [24,25,44]. Since the Au film is too thin to cover the underlying TiO_2(110) substrate, the attenuation of the Ti^{3+}3d peak could be reasonably explained by the

DOI:10.1088/1674-0068/22/04/339-345

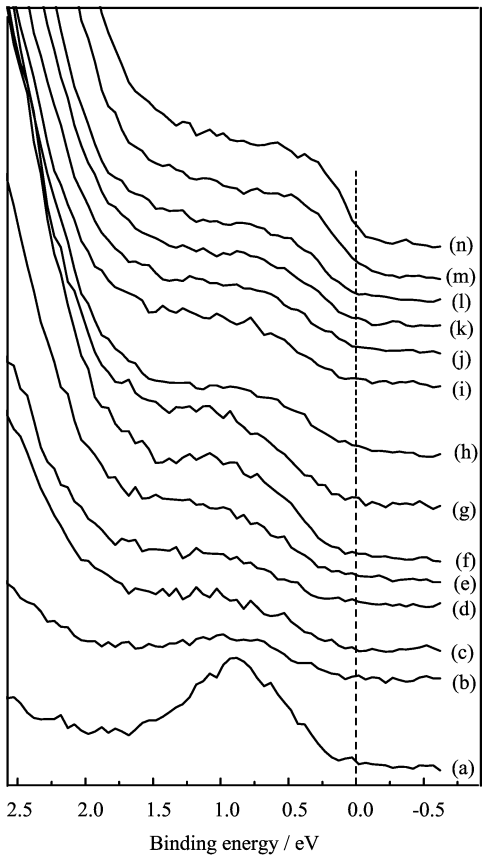

FIG. 4 The valence-band photoemission spectra for Au deposition at room temperature on the r-TiO_2(110) surface with Au thickness of 0, 0.1, 0.3, 0.5, 0.7, 1.0, 1.2, 1.5, 1.7, 2.0, 2.5, 3.0, 5.0, and 0.0 Å for (a)–(n), respectively. The incident photon energy was 28 eV.

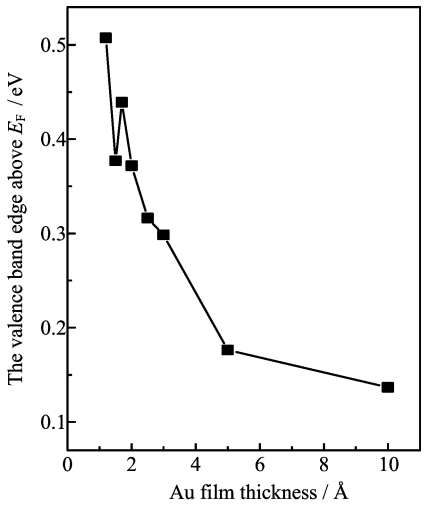

FIG. 5 The valence band edge position of Au clusters as a function of the deposited Au film thickness on the r-TiO_2(110) surface.

charge transfer from the bridging oxygen vacancies on r-TiO_2(110) to Au clusters, which leads to the oxidation of Ti^{3+} to Ti^{4+}. These results also indicate that Au clusters preferentially nucleate on the bridging oxygen vacancies on r-TiO_2(110), agreeing with theoretical calculations [30–33] and STM observations [13]. The Ti3p (excited by hν=150 eV synchrotron-radiation-light) and Ti2p (excited by Mg Kα radiation) XPS features were recorded during the Au growth on r-TiO_2(110), the Ti2p and Ti3p XPS peak intensities decrease with increasing Au thickness, but no distinct binding energy shift was observed for both the Ti2p and Ti3p XPS features as the Ti^{3+} on r-TiO_2(110) was oxidized to Ti^{4+}. This should be due to the massive Ti^{4+} substrate effect. Since Ti^{4+} does not have the 3d electron emission, the Ti^{3+}3d XPS feature is not disturbed by the massive Ti^{4+} in the substrate and thus its change upon the Au growth could be clearly observed.

The Au6s photoemission feature of Au clusters at the initial deposition is more like a discrete peak. With further increasing Au film thickness, the Au6s photoemission feature continuously grows, moves toward lower binding energy, and gradually develops into a band that mixes with the Au5d photoemission feature to form the valence band. These results could be well understood by the fact that the number of Au atoms in a Au cluster increases greatly with increasing cluster size. Similar results have also been reported for Cu growth on α-Al_2O_3(0001) [45] and for Mo growth on the thin Al_2O_3 film [46]. We also plotted the Au6s valence band edge position as a function of the Au film thickness (Fig.5). To completely rule out the likely interference from the Ti^{3+}3d peak and determine the valence band edge with reliable accuracy, we started with the Au film with a thickness of 1.2 Å. It can be seen that the Au6s valence band edge exhibits a similar dependence on the Au film thickness to the Au4f binding energy. The position of the Fermi level of metal nanoparticles plays a decisive role in their ability to interact and activate reactants. The distinguished difference between the Fermi edge position of Au clusters and that of bulk Au implies that Au clusters and bulk Au will exhibit different catalytic behaviors. A nice example is that fine Au nanoparticles are active in activating oxygen at low temperatures whereas bulk Au is not.

Both the SR-PES spectra and the valence-band photoelectron spectra demonstrate that the deposition of 10.0 Å-thick Au film on r-TiO_2(110) does not form Au nanoparticles with the same electronic property as the bulk Au. However, it has been previously reported [23,39] that the deposition of the same thick Au film on the stoichiometric TiO_2(110) surface is enough for Au to exhibit the same $Au4f_{7/2}$ binding energy as the bulk Au. These could be attributed to different growth modes for Au clusters on the stoichiometric and reduced TiO_2(110) surfaces. The potential energy maps for Au atoms on the stoichiometric and reduced TiO_2(110) surfaces showed that the presence of bridging-oxygen vacancies on TiO_2(110) dramatically altered the adsorp-

DOI:10.1088/1674-0068/22/04/339-345

tion and surface diffusion of single Au atoms, and in turn the growth and structure of Au clusters [33]. On the stoichiometric (1×1) surfaces, the Au clusters aggregated into large particles and dominantly covered steps even at room temperature; in contrast, on the reduced (1×2) surfaces, the Au particles were of a smaller size and were highly dispersed on terraces [22]. Campbell and co-workers also reported that, at the same deposition thickness, Au clusters formed on the reduced surface are finer than those on the stoichiometric surface [47].

We also comparatively investigated the thermal stability of Au clusters after depositing the same thickness Au film on s-TiO_2(110) and r-TiO_2(110) surfaces. Figure 6 shows the normalized SR-PES peak intensities of Au4f feature as a function of annealing temperature. Two kinds of Au film thicknesses, 0.5 and 10.0 Å, were chosen. In an attempt to clearly display the variation trend of the Au4f peak intensities as a function of annealing temperature, the Au4f areas at elevated temperatures in Fig.6 were normalized against the respective ones at room temperature on s-TiO_2(110) and r-TiO_2(110). The Au4f peak intensity obviously reduces after annealing at temperatures above 673 and 873 K for 0.5-Å-thick Au film on s-TiO_2(110) and r-TiO_2(110), respectively. When the Au film thickness is 10.0 Å, the obvious reduction of the Au4f peak intensity occurs after annealing at temperatures above 873 and 1073 K, respectively. Upon heating, two processes might result in the attenuation of Au4f SR-PES peak. One is desorption of Au clusters from the surface; the other is the aggregation of Au clusters into large nanoparticles. With a fixed metal amount on the surface, finer particles with a higher dispersion will exhibit a stronger core-level PES peak than larger particles. The stability of Au clusters on oxide surfaces was previously studied by means of thermal desorption spectroscopy. Au cluster was found to desorb from the TiO_2(001)/Mo(100) surface at temperatures higher than 1100 K [48], and from the TiO_x/Mo(112) surface at temperatures higher than 1200 K [12,49], and from a SiO_2 thin film on Mo(110) at 1100 K at low Au coverages [23]. It was also observed that the desorption maximum of Au clusters from a SiO_2 thin film on Mo(110) shifts toward higher temperature with increasing Au coverage [23]. Therefore, we do not consider the desorption of Au clusters from the surface during the course of annealing experiments. It is mostly likely that the aggregation of Au clusters is responsible for the observed attenuation of Au4f SR-PES peak intensities. The results of annealing experiments clearly demonstrate that, with the same deposited Au amount, Au clusters are more thermally stable on r-TiO_2(110) than on s-TiO_2(110), indicating that bridging oxygen vacancies on TiO_2(110) can stabilize the supported Au clusters and hinder the aggregation upon thermal annealing. This agrees well with the previous theoretical calculations [13,30–33]. Meanwhile, deposited on the same TiO_2(110) surface,

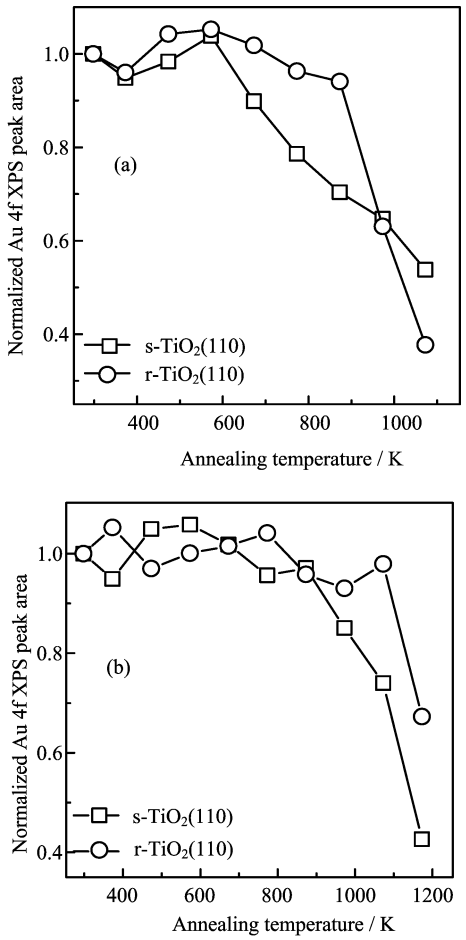

FIG. 6 The normalized Au4f SR-PES peak area of Au clusters on s-TiO_2(110) and r-TiO_2(110) surfaces as a function of the annealing temperature. The deposited Au film thickness is (a) 0.5 Å and (b) 10.0 Å.

large Au nanoparticles seem to be more thermally stable than fine Au nanoparticles. Howard *et al.* have employed XPS and low-energy ion scattering spectroscopy to study the aggregation behavior of Au clusters on TiO_2(110) upon annealing and also observed that fine Au nanoparticles are more prone to aggregate than large Au nanoparticles [25]. However, the difference might also be caused by different sintering mechanisms that fine Au clusters and large Au nanoparticles undergo. Fine Au clusters could facilely diffuse on the surface and coalesce into larger ones whereas large Au nanoparticles could only undergo sintering through the Ostwald ripening mechanism.

IV. CONCLUSION

We have successfully investigated the growth and thermal stability of Au clusters on r-TiO_2(110)-(1×1) by high-resolution photoelectron spectroscopy using synchrotron-radiation-light. Au clusters preferen-

DOI:10.1088/1674-0068/22/04/339-345

tially nucleate on the bridging oxygen vacancies on r-TiO_2(110). Both the Au4f SR-PES results and the valence-band photoelectron spectroscopic results directly prove the occurrence of charge transfer from the bridging oxygen vacancies to Au clusters. With the same Au deposition amount, Au clusters are more thermally stable on the r-TiO_2(110) surface than on the s-TiO_2(110) surface. Meanwhile, on the same surface, large Au nanoparticles are more thermally stable than fine Au nanoparticles.

V. ACKNOWLEDGMENTS

This work was supported by the National Natural Science Foundation of China (No.20773113 and No.20803072), the Hundred Talent Program of Chinese Academy of Sciences, the MOE Program for Changjiang Scholars and Innovative Research Team (No.IRT0756), and the MPG-CAS Partner-group Program.

[1] M. Haruta, Catal. Today **36**, 153 (1997).
[2] T. Hayashi, K. Tanaka, and M. Haruta, J. Catal. **178**, 566 (1998).
[3] M. Haruta, Cattech **6**, 102 (2002).
[4] M. Valden, S. Pak, X. Lai, and D. W. Goodman, Catal. Lett. **56**, 7 (1998).
[5] D. W. Goodman, Catal. Lett. **99**, 1 (2005).
[6] S. Lee, C. Fan, T. Wu, and S. L. Anderson, J. Am. Chem. Soc. **126**, 5682 (2004).
[7] S. Lee, C. Fan, T. Wu, and S. L. Anderson, Surf. Sci. **578**, 5 (2005).
[8] M. S. Chen and D. W. Goodman, Science **306**, 252 (2004).
[9] M. Valden, X. Lai, and D. W. Goodman, Science **281**, 1647 (1998).
[10] M. S. Chen and D. W. Goodman, Catal. Today **111**, 22 (2006).
[11] M. Haruta, T. Kobayashi, H. Sano, and N. Yamada, Chem. Lett. **16**, 405 (1987).
[12] M. S. Chen and D. W. Goodman, Chem. Soc. Rev. **37**, 1860 (2008).
[13] E. Wahlström, N. Lopez, R. Schaub, P. Thostrup, A. Rønnau, C. Africh, E. Lægsgaard, J. K. Nørskov, and F. Besenbacher, Phys. Rev. Lett. **90**, 026101 (2003).
[14] D. Matthey, J. G. Wang, S. Wendt, J. Matthiesen, R. Schaub, E. Lægsgaard, B. Hammer, and F. Besenbacher, Science **315**, 1692 (2007).
[15] X. Lai and D. W. Goodman, J. Mol. Catal. A **162**, 33 (2000).
[16] C. E. J. Mitchell, A. Howard, M. Carney, and R. G. Egdell, Surf. Sci. **490**, 196 (2001).
[17] A. Kolmakov and D. W. Goodman, Catal. Lett. **70**, 93 (2000).
[18] S. Kielbassa, M. Kinne, and R. J. Behm, J. Phys. Chem. B **108**, 19184 (2004).
[19] E. C. H. Sykes, F. J. Williams, M. S. Tikhov, and R. M. Lambert, J. Phys. Chem. B **106**, 5390 (2002).
[20] A. Kolmakov and D. W. Goodman, Chem. Record **2**, 446 (2002).
[21] T. Okazawa, M. Fujiwara, T. Nishimura, T. Akita, M. Kohyama, and Y. Kido, Surf. Sci. **600**, 1331 (2006).
[22] Y. Maeda, T. Fujitani, S. Tsubota, and M. Haruta, Surf. Sci. **562**, 1 (2004).
[23] C. C. Chusuei, X. Lai, K. Luo, and D. W. Goodman, Top. Catal. **14**, 71 (2001).
[24] T. Minato, T. Susaki, S. Shiraki, H. S. Kato, M. Kawai, and K. I. Aika, Surf. Sci. **566-568**, 1012 (2004).
[25] A. Howard, D. N. S. Clark, C. E. J. Mitchell, R. G. Egdell, and V. R. Dhanak, Surf. Sci. **518**, 210 (2000).
[26] L. Zhang, R. Persaud, and T. E. Madey, Phys. Rev. B **56**, 10549 (1997).
[27] T. Okazawa, M. Kohyama, and Y. Kido, Surf. Sci. **600**, 4430 (2006).
[28] R. Meyer, C. Lemire, S. K. Shaikhutdinov, and H. J. Freund, Gold Bull. **37**, 72 (2004).
[29] K. Okazaki, Y. Morikawa, S. Tanaka, K. Tanaka, and M. Kohyama, Phys. Rev. B **69**, 235404 (2004).
[30] Z. X. Yang, R. Q. Wu, and D. W. Goodman, Phys. Rev. B **61**, 14066 (2000).
[31] N. Lopez, J. K. Nørskov, T. V. W. Janssens, A. Carlsson, A. Puig-Molina, B. S. Clausen, and J. D. Grunwaldt, J. Catal. **225**, 86 (2004).
[32] L. M. Molina, M. D. Rasmussen, and B. Hammer, J. Chem. Phys. **120**, 7673 (2004).
[33] D. Pillay and G. S. Hwang, Phys. Rev. B **72**, 205422 (2005).
[34] A. Vijay, G. Mills, and H. Metiu, J. Chem. Phys. **118**, 6536 (2003).
[35] Z. P. Liu, X. Q. Gong, J. Kohanoff, C. Sanchez, and P. Hu, Phys. Rev. Lett. **91**, 266102 (2003).
[36] M. S. Chen and D. W. Goodman, Acc. Chem. Res. **39**, 739 (2006).
[37] F. Cosandey and T. E. Madey, Surf. Rev. Lett. **8**, 73 (2001).
[38] M. S. Chen, Y. Cai, Z. Yan, and D. W. Goodman, J. Am. Chem. Soc. **128**, 6341 (2006).
[39] Z. Q. Jiang, W. H. Zhang, L. Jin, X. Yang, F. Q. Xu, J. F. Zhu, and W. X. Huang, J. Phys. Chem. C **111**, 12434 (2007).
[40] V. E. Henrich, Prog. Surf. Sci. **9**, 143 (1979).
[41] Z. M. Zhang, S. P. Jeng, and V. E. Henrich, Phys. Rev. B **43**, 12004 (1991).
[42] D. C. Lim, I. Lopez-Salido, R. Dietsche, M. Bubek, and Y. D. Kim, Angew. Chem. Int. Ed. **45**, 2413 (2006).
[43] L. Giordano, J. Goniakowski, and G. Pacchioni, Phys. Rev. B **64**, 075417 (2001).
[44] M. S. Chen and D. W. Goodman, Top. Catal. **44**, 41 (2007).
[45] Q. L. Guo and P. J. Møllert, Vacuum **41**, 1114 (1990).
[46] Z. Q. Jiang, W. X. Huang, Z. Zhang, H. Zhao, D. L. Tan, and X. H. Bao, Chem. Phys. Lett. **439**, 313 (2007).
[47] S. C. Parker, A. W. Grant, V. A. Bondzie, and C. T. Campbell, Surf. Sci. **441**, 10 (1999).
[48] C. Xu, W. S. Oh, G. Liu, D. Y. Kim, and D. W. Goodman, J. Vac. Sci. Technol. A **15**, 1261 (1997).
[49] M. S. Chen, K. Luo, D. Kumar, W. T. Wallace, C. W. Yi, K. K. Gath, and D. W. Goodman, Surf. Sci. **601**, 632 (2007).

DOI:10.1088/1674-0068/22/04/339-345